SIMULATIONS OF AIR-WATER TWO-PHASE FLOW IN AN INCLINED PIPE

Juggurnath D.[a], Dauhoo M.Z.[b], Elahee M.K.[a], Khoodaruth A.*[a], Osowade A.E.[c], Olakoyejo O.T.[c], Obayopo S.O.[d] and Adelaja A.O.[c]
*Author for correspondence
[a]Department of Mechanical and Production Engineering, Faculty of Engineering, University of Mauritius, Reduit, Mauritius.
[b]Department of Mathematics, Faculty of Science, University of Mauritius, Reduit, Mauritius.
[c]Department of Mechanical Engineering, University of Lagos, Lagos, Nigeria.
[d]Department of Mechanical Engineering, , Obafemi Awolowo University, Ile-Ife, Nigeria
E-mail: a.khoodaruth@uom.ac.mu

ABSTRACT

Flow patterns depend on the mass flux and phase composition of the flow and also on the inclination angle of the tube. This work analyses the different flow patterns taking place in an inclined tube at 30° numerically. Both upward and downward flows are considered. The simulations of air-water flow in a pipe of diameter $0.051m$ and length $2m$ have been carried out using one-fluid model. The simulated flow patterns are slug, plug, stratified and bubbly flow. The calculated flow regimes are compared with data taken from the well-known Barnea flow pattern map. ANSYS-FLUENT 16.0 is used to solve the mass and momentum equations using second-order upwind scheme. The model takes into account the influence of gravitational force and the surface tension on the flow. A piecewise linear interface reconstruction based on Youngs's VOF is used. The simulation is carried out for the following combinations of superficial air velocities and superficial water velocities of (0.05, 0.1), (1.0,0.5) and (0.5,9.0) at an inclination angle of 30° and of (1.0, 0.1), (12,5) and (1.0,8.0) at an inclination angle of $-30°$. The volume fraction is predicted. To the authors' knowledge, it is the first time that air-water flow as predicted by Barnea flow pattern map is being reproduced numerically and used to validate the VOF method. The results from FLUENT are compared with the experimental data from the well-known Barnea flow pattern map. The model predictions showed good agreement with experimental data obtained at both angles of inclination.

Keywords: water-air flow, inclined pipe, CFD simulations

INTRODUCTION

Multi-phase flow, especially two-phase flow, has widely been studied in the literature, due to its huge number of applications: refrigeration and air-cooling, automotive, power generation, petroleum and chemical industries and many more. An important consideration should be given to flow regimes taking place in two-phase flows, since other flow parameters such as heat transfer coefficient, pressure drop, void fraction, liquid film thickness, force effects, entrainment and the interface between the two-phases highly depend on flow patterns. Researches have classified flow regimes taking place in horizontal, vertical and inclined tubes, based on visual observations. Currently, several flow regime maps exist, constructed from both dimensional (such as mass flow rate and superficial velocity) and dimensionless (such as dimensionless superficial velocity, vapour quality, Weber number and Martinelli parameter) parameters.

NOMENCLATURE

f	[-]	Body forces such as gravity and surface tension
p	[Pa]	Pressure
U_{GS}	[m/s]	Superficial air velocity
U_{LS}	[m/s]	Superficial water velocity
$\vec{u}$	[m/s]	Velocity

Greek characters

ρ	[kg/m^3]	Density
μ	[Pa s]	Viscosity
α	[-]	Volume fraction
σ	[N/m]	Surface tension

Using Volume of Fluid (VOF) methods, Vallée at al, [1] and Frank, [2] simulated slug flows taking place in horizontal tubes. Also, they analysed the slug flow characteristics, namely slug frequency and slug length. Peng and Ling, [3] simulated air-water horizontal flow characteristics using VOF approach of FLUENT, whereby contours of density mixture for slug-annular, annular, bubble, slug and churn flow are given. Based on Baker's flow regime map in [4], De Schepper et al., [5] and Imada et al., [6] simulated flow regimes numerically using Piecewise Linear Interface Calculation (PLIC) approach. The former one reproduced the flow regimes occurring in a horizontal tube. Imada et al. used Youngs' VOF method to reproduce stratified, horizontal plug and vertical slug flow patterns. The above literature review demonstrates that most of the available numerical simulations of two-phase flow patterns are for horizontal tubes. However through experiments, many authors emphasized that the inclination angle of the tube is a vital parameter that should be considered. Many studies on condensation ([7]-[10]) demonstrated an optimum inclination angle of 15° to 30°,

downward flow to the highest heat transfer coefficient. It should be noted that the optimum angle in relation to heat transfer for two phase flow consisting of water-air has not been investigated. Heuristically, we choose an angle of 30° to replicate and understand air-water flow patterns in both upward and downward tube orientations. To the authors' knowledge, till date, there is no work in which the VOF model has been validated with Barnea flow pattern maps. Therefore, the objective of this paper is to numerically simulate the flow patterns resulting in a 30° upward and downward flow. Upward and downward flows will be represented by $'+'$ and $'-'$ signs respectively. The experimental data, most precisely the superficial velocities of water and air are retrieved from the well-used Barnea flow pattern map, [11].

The next section illustrates the flow pattern map used and a brief explanation on flow regimes is presented.

FLOW PATTERN MAPS

The Barnea flow pattern map, [11] predicts transitions between smooth-stratified, stratified-wavy, annular, annular-wavy, churn, slug, elongated bubble (plug), bubbly and dispersed bubbly flows for a range of inclination angles. The corresponding flow pattern maps for inclination angles of 30° and −30° are illustrated in Figure 1 and 2. The significance of the symbols is explained in Figure 3. Widely used in the literature, the flow regimes on Barnea map were determined and established in a tube with diameter $0.051m$. For simplicity in this work, smooth-stratified and stratified-wavy are grouped under stratified flow. Similarly, annular and annular-wavy are considered under annular flow and bubbly and dispersed bubbly under bubbly flow.

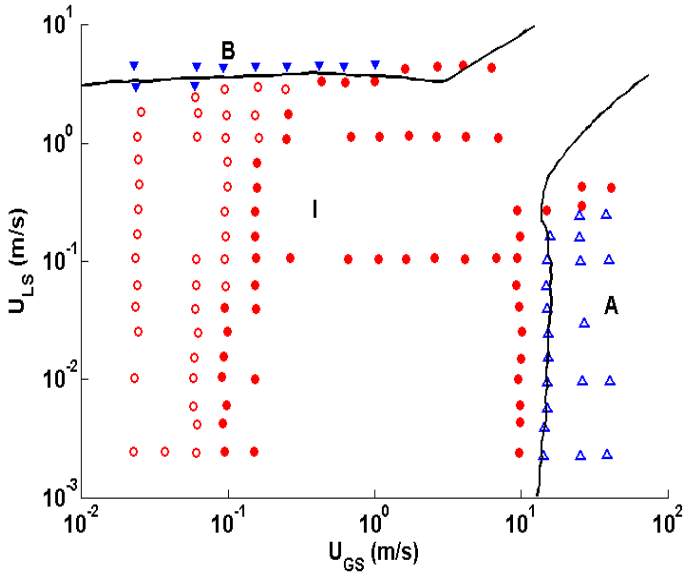

Figure 1. Barnea flow pattern map for a 0.051 m diameter tube at an inclination angle of 30°. (B: Bubbly, I: Intermittent, A: Annular) [11]

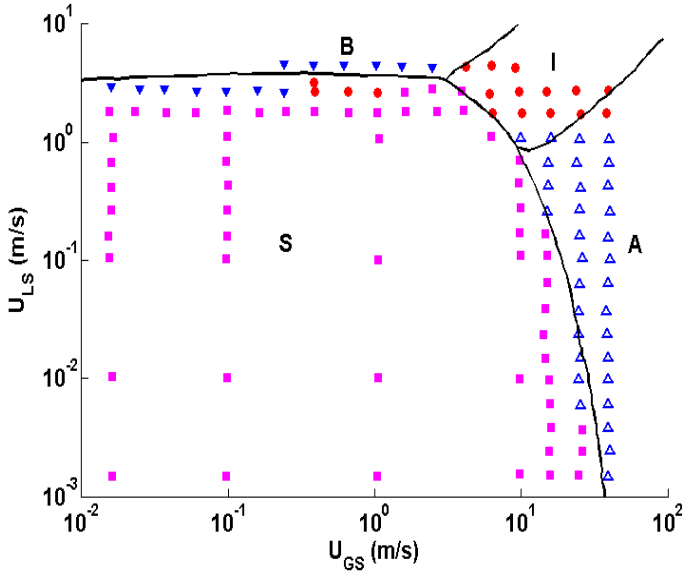

Figure 2. Barnea flow pattern map for a 0.051 m diameter tube at an inclination angle of −30°. (B: Bubbly, S: Stratified, I: Intermittent, A: Annular) [11]

Figure 3. Significance of symbol used on Barnea flow pattern map.

A short description on different flow regimes is given below:

Stratified flow: At low liquid and gas velocities, there is a complete separation of liquid and gas with an undisturbed horizontal interface. The gas flows at the top of the tube while a thick layer of liquid flows at the bottom of the tube, due to the high influence of gravity. When the interface is affected by waves, the wavy flow is said to occur. However, the waves do not arrive at the top of the tube. They wet the sides of the tube leaving thin liquid films.

Intermittent flow: Decreasing the gas velocity, the amplitude of the waves is enough to wash the top of the tube only. Intermittent flow is subdivided into two categories: Plug and slug flows.

Plug flow: The presence of long elongated bubbles separate the liquid plugs. The diameter of the bubbles are small enough for the liquid phase to flow continuously along the tube.

Slug flow: The diameter of the bubbles increases until it equals the diameter of the tube. A thin liquid film is allowed to flow between the bubbles and the tube wall. These bubbles are also known as Taylor bubbles. In the vertical upward flow, the thin liquid film flows downward with the influence of gravity, while the net

flow of fluid is upward.

Annular flow: At very high gas rate, the annular flow is observed. The liquid is expelled from the centre allowing gas to flow continuously along the tube core while the liquid film flows around the perimeter of the tube. Due to the high interfacial shear stress and negligible gravitational force, a uniform liquid film is observed.

Bubbly flow: At lower gas velocities, bubbly flow is observed where numerous small bubbles are dispersed in the liquid.

The next section gives an overview of VOF method.

VOLUME OF FLUID (VOF) APPROACH

Volume of fluid methods belong to the Eulerian-Eulerian category, where a fixed grid system is used to represent the motion of the fluids. The fluids go through a particular control volume and are continuously replaced in time. VOF models are used to simulate two or more immiscible fluids, by solving a single set of momentum equations as given below throughout the domain.

$$\frac{\partial}{\partial t}(\rho\vec{u}) + \nabla\cdot(\rho\vec{u}\vec{u}) = -\nabla\cdot p + \nabla\cdot\mu(\nabla\vec{u} + \nabla\vec{u}^T) + f \quad (1)$$

which should satisfy the conservation of mass,

$$\frac{\partial}{\partial t}(\rho) + \nabla\cdot(\rho\vec{u}) = 0. \quad (2)$$

This method keeps track of the volume fraction of a certain fluid, k in each grid cell be defining a fractional volume function, α where

$$\alpha = \begin{cases} 1, \text{ if there is fluid } k \text{ in the cell,} \\ 0, \text{ if there is no fluid } k \text{ in the cell,} \\ 0 < \alpha < 1, \text{ if there is an interface in the cell.} \end{cases} \quad (3)$$

Hence, the resulting velocity field from Eq.(1) is shared among the phases through mixture properties, which depend on volume fractions. These properties are determined as below:

$$\rho = \alpha\rho_{water} + (1-\alpha)\rho_{air} \text{ and } \mu = \alpha\mu_{water} + (1-\alpha)\mu_{air} \quad (4)$$

To track the position of the interface, the volume fraction is calculated and updated using the advection equation given by

$$\frac{\partial}{\partial t}\alpha + (\vec{u}\cdot\nabla)\alpha = 0. \quad (5)$$

The solution of only one equation makes volume of fluid approach very computationally friendly and therefore requires minimal storage. Simple and accurate, VOF method has been chosen due to its mass preserving nature and its ability to deal with sharp topological changes. [12]

The different approaches to VOF simulations can be classified into 3 categories:

1. Donor-Acceptor schemes
2. High Order Differencing schemes
3. Line techniques

A description of the different VOF approaches is given below:

Donor-Acceptor schemes

Hirt and Nichols VOF method

The VOF method was first deduced by Hirt and Nichols [13]. In the nature of SLIC, a line technique approach, the Hirt and Nichols method reconstructs the interface parallel to one of the coordinate axes. However, nine neighbouring cells are used to estimate the surface normals in a particular cell. The interface is then represented as a horizontal or vertical line in a cell, depending on the magnitude of the surface normals. Based on the orientation of the reconstructed interface, upwind or donor-acceptor scheme is used to calculate the transferred flux from the donor cell. The flux $F_{i+\frac{1}{2},j}$ across the face $(i+\frac{1}{2}, j)$ with face velocity $u_{i+\frac{1}{2},j}$ is defined as

$$F_{i+\frac{1}{2},j} = \triangle y\{min[\alpha_{i,j}\triangle x, u_{i+\frac{1}{2},j}\alpha_{i+1,j}\triangle t + max(0, u_{i+\frac{1}{2},j}(1.0-\alpha_{i+1,j})\triangle t - (1.0-\alpha_{i,j})\triangle x)]\} \quad (6)$$

Therefore, upwind scheme are used to calculate fluxes which are parallel to the reconstructed interface while donor-acceptor scheme is used for fluxes perpendicular to the reconstructed interface.

High order Differencing schemes

Flux-Corrected Transport (FCT) method

The flux-corrected transport method is a combination of low and high order fluxes in order to eliminate the numerical diffusion and instability of the low and high order schemes. FCT approach was first designed by Boris and Book [14] and was the extended to multidimensional by Zalesak [15]. Rudman [16] used the concept of FCT to develop a direction-split algorithm for volume tracking. In this method, a low order flux, F^L based on upwind scheme is used to determine an intermediate value of the volume

fraction, α^* as given below:

$$\alpha_i^* = \alpha_i^n - \frac{1}{\triangle x}\left(F^L_{i+\frac{1}{2}} - F^L_{i-\frac{1}{2}}\right). \tag{7}$$

A high order flux based on first-order downwind scheme is used to determine the anti-diffusive flux, F^A.
The anti-diffusive flux is then limited with factors, κ to obtain the values of the volume fraction at the next time level.

$$\alpha_i^{n+1} = \alpha_i^* - \frac{\kappa_{i+\frac{1}{2}} F^A_{i+\frac{1}{2}} - \kappa_{i-\frac{1}{2}} F^A_{i-\frac{1}{2}}}{\triangle x}. \tag{8}$$

Compressive Interface Capturing Scheme for Arbitrary meshes (CICSAM)
Introduced by Ubbink and Issa [17], CICSAM limits the volume fraction by switching between different differencing schemes in order to preserve boundedness. The determination of the volume fraction is based on the Normalised Variable Diagram (NVD). The CICSAM scheme can mathematically b written as

$$\tilde{\alpha} = \gamma \tilde{\alpha}_{CBC} + (1-\gamma)\tilde{\alpha}_{UQ} \tag{9}$$

where $\tilde{\alpha}$ is a normalised volume fraction and γ is a weighting factor.
The ultimate-quickest scheme gives $\tilde{\alpha}_{UQ}$ as

$$\tilde{\alpha}_{UQ} = \begin{cases} min\{\frac{8c\tilde{\alpha}_D+(1-c)(6\tilde{\alpha}_D+3)}{8}, \tilde{\alpha}_{CBC}\}, & \text{when } 0 \le \tilde{\alpha}_D \le 1 \\ \tilde{\alpha}_D, & \text{when } \tilde{\alpha}_D < 0, \tilde{\alpha}_D > 1. \end{cases} \tag{10}$$

and the local boundedness criteria is preserved with the upper-bound of the convection boundedness criteria (CBC) defined as

$$\tilde{\alpha}_{CBC} = \begin{cases} min\{\frac{\tilde{\alpha}_D}{c}, 1.0\}, & \text{when } 0 \le \tilde{\alpha}_D \le 1 \\ \tilde{\alpha}_D, & \text{when } \tilde{\alpha}_D < 0, \tilde{\alpha}_D > 1. \end{cases} \tag{11}$$

where $\tilde{\alpha}_D$ is the normalised volume fraction in the donor cell and c is the Courant number.

According to [18], CICSAM is suited for multiphase flows with high difference in viscosities.

Modified High Resolution Interface Capturing (HRIC)
Very similar to CICSAM, the HRIC approach, proposed by Muzaferija [19] blends upwind and downwind differencing schemes. The normalised volume fraction is given by

$$\tilde{\alpha} = \begin{cases} \tilde{\alpha}^{**}, & \text{for } c < 0.3, \\ \tilde{\alpha}_D, & \text{for } c > 0.7, \\ \tilde{\alpha}_D + (\tilde{\alpha}^{**} - \tilde{\alpha}_D)\frac{0.7-c}{0.7-0.3}, & \text{for } 0.3 \le c \le 0.7 \end{cases} \tag{12}$$

where a blending factor γ is introduced to cause a gradual switch between the schemes resulting in

$$\tilde{\alpha}^{**} = \gamma\tilde{\alpha}^* + \tilde{\alpha}_D(1-\gamma) \tag{13}$$

and $\tilde{\alpha}^*$ results from both upwind and downwind schemes,

$$\tilde{\alpha}^* = \begin{cases} \tilde{\alpha}_D, & \text{for } \tilde{\alpha}_D < 0, \tilde{\alpha}_D > 1 \\ 2\tilde{\alpha}_D, & \text{for } 0 \le \tilde{\alpha}_D < \frac{1}{2}, \\ 1, & \text{for } \frac{1}{2} \le \tilde{\alpha}_D \le 1 \end{cases} \tag{14}$$

The modified HRIC of FLUENT is more accurate than the other face flux scheme available in the commercial software. [18]

Line techniques

Simple Line Interface Calculation (SLIC)
Introduced by Noh and Woodward [20], the SLIC method is first-order accurate. Based on direction-split algorithm, only neighbouring cells in a particular sweep direction are used to reconstruct the interface, which is parallel to one of the coordinate axes. Therefore, for each direction sweep, the interface cells may have different representations. Figure 4 below shows the possible interface representation by SLIC.

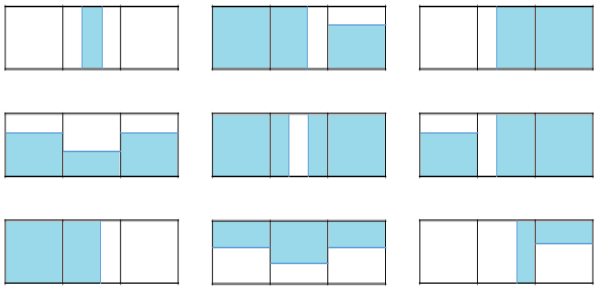

Figure 4. The nine possible ways SLIC reconstructs the interface. The shaded area represents the fluid.

Youngs's VOF method
Instead of aligning the reconstructed interface with a coordinate axis, Youngs's VOF method [21] calculates the angle β the interface makes with the x-axis by first determining the normal vector η to the interface segment,

$$tan\,\beta = -\frac{\eta^x}{\eta^y} \text{ where } -\pi < \beta < \pi. \tag{15}$$

where

$$\eta^x = \frac{1}{\triangle x}[\alpha_{i+1,j+1} + 2\alpha_{i+1,j} + \alpha_{i+1,j-1} - \alpha_{i-1,j+1} - 2\alpha_{i-1,j} - \alpha_{i-1,j-1}] \tag{16}$$

and

$$\eta^y = \frac{1}{\triangle y}[\alpha_{i+1,j+1} + 2\alpha_{i,j+1} + \alpha_{i-1,j+1} - \alpha_{i+1,j-1} - 2\alpha_{i,j-1} - \alpha_{i-1,j-1}]. \quad (17)$$

Depending on the angle θ,

$$tan\,\theta = \frac{\triangle x}{\triangle y} tan\,\beta \quad (18)$$

the interface type and orientation is established. The amount of fluid being advected through each face is then calculated to determine the volume fraction in each cell. Rudman [16] investigated the accuracy and efficiency of SLIC, Hirt & Nichols, FCT-VOF and Youngs's VOF approaches and concluded that Youngs's VOF technique outstands the other mentioned ones. Figure 5 by [22] gives an excellent illustration of the use of both SLIC and PLIC. The accuracy of PLIC compared to SLIC approach is noted.

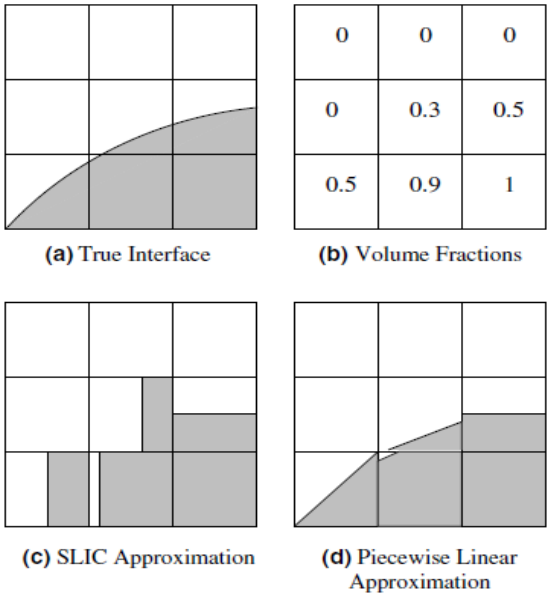

Figure 5. The interface in (a) is reconstructed by VOF methods which stores volume fractions associated with the interface in each cell, as shown in (b). The interface is approximated by two interface reconstruction methods, SLIC in (c) and PLIC in (d). [22]

This approach is known as "Geo-Reconstruct" in ANSYS-FLUENT. In this paper, the Geo-Reconstruct method is used to determine the interface since it is the most accurate one in FLUENT.

NUMERICAL SIMULATIONS

Tube geometry and operating conditions

The flow domain was constructed on Design Modeller and meshed on Meshing. The diameter and length of the tube are $0.051m$ and $2m$ respectively. It should be noted that the tube was inclined at an angle of 30°, either downward or upward and this criteria has been included in the solver. Water and air were introduced at 2 different inlets. The setup of the tube can be assumed to consist of four sections, namely, water inlet, air inlet, pipe outlet and test section as shown in Figure 6.

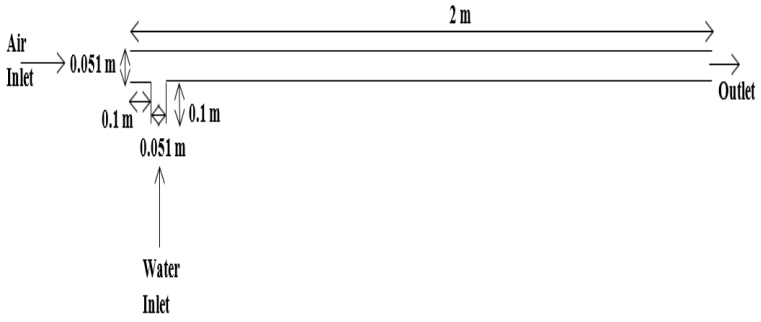

Figure 6. Schema of tube and dimensions

The domain consisted of 10,500 quadrilateral cells, which was chosen to account for surface tension more accurately, as illustrated in Figure 7. The smallest mesh size was $0.00255m$, which is refined enough to capture the features of the flow regimes.

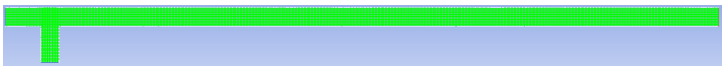

Figure 7. Meshing of tube

Boundary conditions

Tables 1 and 2 give the inlet superficial velocities of water and air for each flow regimes in both upward and downward tube orientation respectively. These parameters are obtained from Barnea flow pattern maps, Figures 1 and 2. At both inlets, the fluid pressure is set to 101,325 Pa. The tube wall is stationary and no-slip boundary condition is imposed. At the pipe outlet, pressure outlet condition has been employed.

Table 1. Operating conditions for air-water flow in 30° inclined tube. [11]

Flow pattern	Superficial air velocity (m/s)	Superficial water velocity (m/s)
Plug flow	0.05	0.1
Slug flow	1.0	0.5
Bubbly flow	0.5	9.0

The physical properties of water and air are given in Table 3 below.

Table 2. Operating conditions for air-water flow in $-30°$ inclined tube. [11]

Flow pattern	Superficial air velocity (m/s)	Superficial water velocity (m/s)
Stratified flow	1.0	0.1
Slug flow	12	5
Bubbly flow	1.0	8.0

Table 3. Physical conditions of water and air

	$\rho\ (kg/m^3)$	$\mu\ (Pa\ s)$	$\sigma\ (N/m)$
Water	998.2	0.001003	0.071904
Air	1.225	0.000017894	-

Methodology

The flow solver used was ANSYS FLUENT which uses a finite volume method to convert the governing partial differential equations into a system of discrete algebraic equations by discretising the computational domain. The details of the method were explained by Patankar, [23]. The simulations were carried out under transient condition. The non-iterative time advancement scheme is chosen to increase speed and efficiency of the computations. Moreover, the solver was run in 2-dimensional mode. The residual tolerance was set to 0.0001 for all variables to indicate convergence of the calculations. The VOF model is chosen for the numerical simulation of air-water flow. The tube is initially filled with water. Water and air are then introduced into the pipe at a particular water and air superficial velocities respectively. The surface tension along the interface is accounted through the Continuum Surface Force (CSF) model, as proposed by Brackbill et al, [24]. The surface force is converted to a volume force using the divergence theorem and is added as a source term in the momentum equation. To account for turbulence effects of the flow, the realizable $k-\varepsilon$ model is chosen. The model transport equations for the turbulent kinetic energy k and its rate of dissipation ε are given as

$$\frac{\partial}{\partial t}(\rho k)+\frac{\partial}{\partial t}(\rho k u_j)=\frac{\partial}{\partial x_j}\left[\left(\mu+\frac{\mu_t}{\delta_k}\right)\frac{\partial k}{\partial x_j}\right]+G_k-\rho\varepsilon, \quad (19)$$

$$\frac{\partial}{\partial t}(\rho\varepsilon)+\frac{\partial}{\partial t}(\rho\varepsilon u_j)=\frac{\partial}{\partial x_j}\left[\left(\mu+\frac{\mu_t}{\delta_\varepsilon}\right)\frac{\partial \varepsilon}{\partial x_j}\right]+\rho C_1 S\varepsilon-\rho C_2\frac{\varepsilon^2}{k+\sqrt{\nu\varepsilon}}, \quad (20)$$

where $C_1 = max[0.43, \frac{\eta}{\eta+5}]$, $\eta = S\frac{k}{\varepsilon}$, $S=\sqrt{2S_{ij}S_{ij}}$, S_{ij} being the mean rate of strain tensor, $C_{1\varepsilon}=1.44$, $C_2=1.9$, $\delta_k=1.0$, $\delta_\varepsilon=1.2$. G_k, ν and μ_t are the generation of turbulent kinetic energy due to the mean velocity gradient, the kinematic viscosity and turbulent viscosity respectively. [18]

The conservation of pressure and velocity is effected by solving the momentum and pressure equation using the PISO pressure-velocity coupling scheme. The Least Squares cell based method is used to evaluate the gradient. The PRESTO scheme is used to determine the pressure interpolation. A second order upwind scheme is used to solve the momentum equations and first order upwind scheme is used for the determination of the two turbulence equations. Since piecewise linear interface reconstruction approaches give best interfaces, Geo-Reconstruct method which is based on Youngs's VOF is chosen to determine the volume fraction in each cells, [16], [18].

RESULTS AND DISCUSSION

As mentioned precedingly, the simulations results of flow regimes are for an inclined tube at 30°. According to Barnea flow chart, the resulting flow regimes are compared in both upward and downward directions. The following pictures of flow patterns show contours of mixture density flowing from left to right. Since the mixture density is related to the volume fraction in each cell, the phase composition is easily observed in the tube. The red colour represents the distribution of pure water (998.2 kg/m^3) while the dark blue colour represents the distribution of pure air (1.225 kg/m^3) as illustrated in Figure 8.

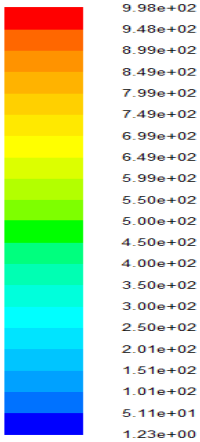

Figure 8. A colourbar representing the mixture density.

Bubbly Flow

Figures 9 and 10 show bubbly flows in upward and downward directions respectively. At the beginning of the bubbly flow in the upward direction, it has been noted that the bubbles occupy only the upper part of the tube. With time, a large cross-section of the pipe is occupied by the bubbles. It should be noted that the bubbles are quite dispersed in the upward bubbly flow. Regarding the downward direction, since the bubbles flow in the opposite direction to the flow direction, shearing and degeneration of bubbles into smaller ones is observed. This results in a higher bubble dispersion when compared to upward flow, as illustrated in Figures 9 and 10.

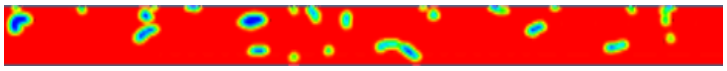

Figure 9. A section of the tube showing bubbly flow in upward direction

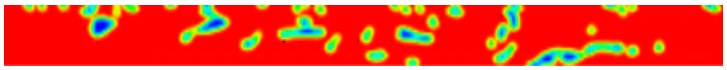

Figure 10. A section of the tube showing bubbly flow in downward direction

Slug Flow

The slug flow of water and air taking place in an upward and downward directions are illustrated in Figures 11 and 12. When compared to the downward slug flow, a distinctive trailing end can be noted in the upward slug flow. Table 1 and 2 show that bubble-to-slug transition occurs at much higher superficial velocities in the downward flow than in the upward flow. The most surprising one is the superficial air velocity that shifts from 1 in upward to 12 in downward. An explanation to this shift is the shearing of bubbles that occur in downward flow. The liquid slugs can clearly be identified in the downward flow. The size of the slugs equals the tube diameter, allowing a thin water film to flow between the air pockets and the wall, which characterises the slug flow exactly.

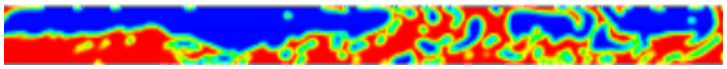

Figure 11. A section of the tube showing slug flow in upward direction

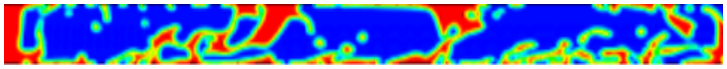

Figure 12. A section of the tube showing slug flow in downward direction

Plug Flow

It can easily be noticed from Barnea flow pattern map, that plug flow takes place in upward flows only. Figure 13 shows the elongated bubbles in air-water flow in 30° inclined tube. The diameter of the air pockets distinguishes the plug and the slug flow, as seen in Figure 13 and 11. Again, it should be noted that the elongated bubbles occupy the upper part of the tube in upward flow.

It is clear that besides flow rates, fluid properties and pipe diameter, transient flow pattern transitions also depend on time and position from the inlet, [25]. Despite plug flow not being mentioned on the downward flow chart, a bubbly-plug transition was observed in downward direction, as illustrated in Figure 14. The high concentration of elongated bubbles (plug) in Figure 14 distinguishes the bubble-plug transition from the bubbly flow in Figures 9 and 10. The condition for the bubbly-plug transition is the inlet superficial velocities of downward bubbly flow and a longer time period.

Figure 13. A section of the tube showing plug flow in upward direction

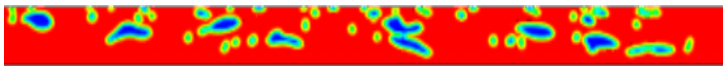

Figure 14. A section of the tube showing plug flow in downward direction

Stratified flow

It can easily be seen from Barnea flow pattern map that stratified flows occur mostly in downward direction. Figure 15 reflects the simulated stratified flow. It should be noted that the interface is smooth. However for these superficial velocities, Barnea flow chart as in Figure 2 expects a stratified-wavy flow.

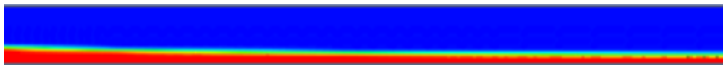

Figure 15. A section of the tube showing stratified flow in downward direction

CONCLUSION

Computational fluid dynamics study has been carried out to simulate air-water flow patterns in a 30° upward and downward inclined tube, as predicted by Barnea flow pattern maps. Volume of Fluid approach has been used to track the interface between air-water flow and a piecewise linear interface reconstruction method has been used to reproduce the interface. The simulated flow patterns are slug, plug, stratified and bubbly flow. In each case, where possible, both the resulting upward and downward flow regimes have been compared. The influence of gravitational force and surface tension has been included. All of mentioned flow regimes have successfully been modeled using ANSYS-FLUENT 16.0 and the simulations showed good agreement with the expected flow regimes. We are currently working on the annular flow regime for air-water flow.

ACKNOWLEDGMENT

This paper is part of a research entitled "Harnessing unsteady phase-change heat exchange in high-performance concentrated solar power systems" funded by the Royal Society - DFID (UK) under the Africa Capacity Building Initiative. The authors thank also all members of the Consortium awarded a grant under the latter Initiative, namely, Imperial College London, University of Pretoria and University of Lagos. The authors are grateful for the help of Mr. Soopee Asif, Mr. Mungur Atish and Ms. Poorun Yashna of the University of Mauritius.

REFERENCES

[1] Vallée, C., Höhne, T., Prasser, H.M., and Sühnel, T., Experimental investigation and CFD simulation of horizontal stratified two-phase flow phenomena, *Nuclear Engineering and Design*, Vol. 238, 2008, pp. 637-646

[2] Frank, T., Numerical simulation of slug flow regime for an air-water two-phase flow in horizontal pipes, *Proceedings of the 11th International Topical Meeting on Nuclear Reactor Thermal-Hydraulics (NURETH-11)*, Avignon, France, October. 2005.

[3] Peng, H., and Ling, X., Computational fluid dynamics modelling on flow characteristics of two-phase flow in micro-channels, *Micro & Nano Letters* Vol. 6, 2011, pp. 372-377

[4] Baker, O., Design of pipelines for the simultaneous flow of oil and gas, *Fall Meeting of the Petroleum Branch of AIME*, Society of Petroleum Engineers, 1953.

[5] De Schepper, S. CK., Heynderickx, G. J. and Marin, G. B., CFD modeling of all gasliquid and vaporliquid flow regimes predicted by the Baker chart, *Chemical Engineering Journal*, Vol. 138, 2008, pp. 349-357

[6] Imada, F. H. J., Saltara, F. and Balio, J. L., Numerical simulation of stratified, horizontal plug and vertical slug flow patterns, 2013

[7] Lips, S., and Meyer, J. P., Experimental study of convective condensation in an inclined smooth tube. Part I: Inclination effect on flow pattern and heat transfer coefficient, *International Journal of Heat and Mass Transfer*, Vol. 55, 2012, pp. 395-404

[8] Meyer, J. P., Dirker, J. and Adelaja, A. O., Condensation heat transfer in smooth inclined tubes for R134a at different saturation temperatures, *International Journal of Heat and Mass Transfer*, Vol. 70, 2014, pp. 515-525

[9] Lyulin, Y., Marchuk, I., Chikov, S., and Kabov, O., Experimental study of laminar convective condensation of pure vapor inside an inclined circular tube, *Microgravity Science and Technology*, Vol. 23, 2011, pp. 439-445

[10] Lips, S., and Meyer, J. P., Effect of gravity forces on heat transfer and pressure drop during condensation of R134a, *Microgravity Science and Technology*, Vol. 24, 2012, pp. 157-164

[11] Barnea, D., A unified model for predicting flow-pattern transitions for the whole range of pipe inclinations, *International Journal of Multiphase Flow*, Vol. 13, 1987, pp. 1-12

[12] Srinivas, V.L., Stof interface tracking and capturing methods. *Diss. Indian Institude of Technology, Madras*, 2016.

[13] Hirt, C.W., and Nichols., B.D., Volume of fluid (VOF) method for the dynamics of free boundaries, *Journal of computational physics*, Vol. 39, 1981, pp. 201-225

[14] Boris, J.P., and Book, D.L., Flux-corrected transport. I. SHASTA, a fluid transport algorithm that works, *Journal of computational physics*, Vol. 11, 1973, pp. 38-69

[15] Zalesak, S.T., Fully multidimensional flux-corrected transport algorithms for fluids, *Journal of computational physics*, Vol. 31, 1979, pp. 35-362

[16] Rudman, M., Volume-tracking methods for interfacial flow calculations, *International journal for numerical methods in fluids*, Vol. 24, 1997, pp. 671-691

[17] Ubbink, O., and Issa., R.I., A method for capturing sharp fluid interfaces on arbitrary meshes, *Journal of Computational Physics*, Vol. 153, 1999, pp. 26-50

[18] ANSYS, FLUENT, 6.3 User Guide, ANSYS, 2006

[19] Muzaferija, S., Peric, M., Sames, P.C., and Schellin, T.E., A two-fluid Navier-Stokes solver to simulate water entry, *Proc. of the 22nd Symp. on Naval Hydro*, 1998

[20] Noh, W.F., and Woodward, P., SLIC (simple line interface calculation), *Proceedings of the Fifth International Conference on Numerical Methods in Fluid Dynamics*, Twente University, Enschede, Springer Berlin Heidelberg, 1976.

[21] Youngs, D.L., Time-dependent multi-material flow with large fluid distortion, *Numerical methods for fluid dynamics*, Vol. 24, 1982, pp. 273-285

[22] Pilliod, J.E., and Puckett, E.G., Second-order accurate volume-of-fluid algorithms for tracking material interfaces, *Journal of Computational Physics*, Vol. 199, 2004, pp. 465-502.

[23] Patankar, S., Numerical heat transfer and fluid flow, *CRC press*, 1980

[24] Brackbill, J.U., Kothe, D.B., and Zemach. C., A continuum method for modeling surface tension, *Journal of computational physics*, Vol. 100, 1992, pp. 335-354

[25] Tong, L.S., and Tang., Y.S., Boiling heat transfer and two-phase flow. *CRC press*, 1997.